Bioconjugate Chemistry

Article

pubs.acs.org/bc

Synthesis, Biological Evaluation, and *in Vivo* Imaging of the first Camptothecin–Fluorescein Conjugate

Arnaud Chevalier,[†] Martine Dubois,[‡,§] Vadim Le Joncour,[‡,§] Sébastien Dautrey,[†] Céline Lecointre,[‡,§] Anthony Romieu,[†] Pierre-Yves Renard,[†] Hélène Castel,*[,‡,§] and Cyrille Sabot*[,†]

[†]Normandie University, COBRA, UMR 6014 and FR 3038; University of Rouen; INSA of Rouen; CNRS, 1 rue Tesnière 76821 Mont-Saint-Aignan, Cedex, France

[‡]Inserm U982, Laboratory of Neuronal and Neuroendocrine Communication and Differentiation (DC2N), Astrocyte and Vascular Niche, Institute of Research and Biomedical Innovation (IRIB), PRES Normandy University, University of Rouen, 76821 Mont-Saint-Aignan Cedex, France

[§]North-West Cancéropole (CNO), 59008 Lille Cedex, France

Supporting Information

ABSTRACT: The first synthesis and photophysical properties of a fluorecently labeled camptothecin derivative, namely, camptothecin-FI (CPT-FI), an antitumoral agent that targets topoisomerase I, are reported. The preparation of this fluorescent conjugate is based on a highly convergent and flexible approach which enables the rapid chemical modification of the AB ring system of this fragile pentacyclic alkaloid, aimed at introducing an anchoring point to graft the fluorophore. The selection of a fluorescein analogue as the reporter group has enabled us to get the first green-emitting CPT conjugate exhibiting valuable spectral properties and retaining biological properties of native CPT. Indeed, in biological models, i.e., glioma cell lines U87 and/or T98, the kinetics of cell endocytosis, as well as the efficacy of CPT-FI were compared to those of CPT. CPT-FI fluorescence was measured in the cytosolic compartment of T98 glioma cells from 5 min treatment and remained detectable until 48 h. As CPT, CPT-FI drastically inhibited glioma growth and cell cycle but exhibited a reduced affinity as compared to the native CPT. *In vivo* and *ex vivo* imaging studies of CPT-FI intratumoraly injected into a model of NIH-3T3 murine tumor xenografts in nude mice, showed accumulation around the injected site area, which is very promising to target tumors and follow biodistribution *in vivo*.

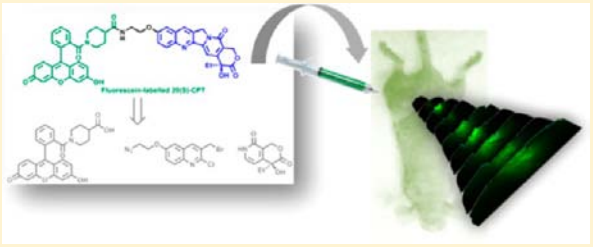

INTRODUCTION

Since its first discovery in 1966,[1] the pentacyclic alkaloid 20(*S*)-camptothecin has emerged as an important lead compound in the field of anticancer drug development. CPT acts by stabilizing the DNA-topoisomerase I binary complex and enhancing apoptosis through blocking the advancement of replication forks.[2] Also, CPT and its numerous derivatives developed over the years display various antitumor activities in a wide range of cancers, such as ovarian and lung (topotecan), colon (irinotecan), or brain (gimatecan and belotecan).[3−5] Despite significant progress, residual secondary effects are still observed, such as, for example, hematological toxicity, headache, fever, and fatigue, associated with the CPT-based chemotherapy. Fluorescent labeling of biomolecules or bioactive compounds is a common way to gain insights into either unwanted organism–drug interactions or pharmacological mechanisms.[6−8] However, despite the number of questions concerning the pharmacokinetic, real access, and penetration in the tumor and the number of side effects of usual chemotherapy (as well as new targeted therapies), strategies for fluorescently labeling of cancer therapeutic drugs have scarcely been developed until now. Thus, we propose here the first strategy to develop original imaging tools, adapted to *in vivo* imaging of the small animal, but also to study mechanisms of action of molecules at the cellular level within tumors (role in apoptosis, proliferation, and vascularization) and in healthy tissues.

Despite the overwhelming number of CPT analogues reported in the literature over the past decade, none of them have already been directly modified[9] with a fluorescent reporter group.[10−12] This can be mainly explained to the absence of a suitable bioconjugatable reactive handle within this pentacyclic alkaloid structure whose derivatization would not drastically affect its biological activity.[13] In addition, the facile hydrolysis of its lactone moiety represents a challenging bioconjugation issue especially for considering further functionalization of this fragile molecular scaffold. Although most CPT derivatives exhibit a natural and strong blue fluorescence, their absorption and emission spectra (e.g., shape, intensity, and wavelength) are highly dependent on the analogue considered and the stability of their crucial E-ring lactone. Indeed, under physiological

Received: September 21, 2012
Revised: June 7, 2013
Published: June 10, 2013

dx.doi.org/10.1021/bc3005304 | *Bioconjugate Chem.* 2013, 24, 1119−1133

conditions, the lactone ring of CPT is rapidly hydrolyzed into the usually less fluorescent and physiologically active carboxylate form.[14−16] Even if the intrinsic fluorescence properties of CPT could be compatible with *in vitro* bioassays,[17] more challenging bioanalytical applications focusing on the tracking of biological events (following administration of this bioactive compound) *in cellulo* or *in vivo* could not be easily implemented due to the blue light absorption and scattering by the biological matrix and the background signal from cellular autofluorescence.[18] Thus, it is essential to dispose of a reliable fluorescent chemical reporter conveniently link to the bioactive alkaloid, to efficiently track the biological processes, whatever the analogues considered and the proportion of its lactone form in biological media. Consequently, in this present work, we wish to provide a general framework to access a fluorescently labeled CPT in order to validate the possibility of fluorescently modified chemotherapy (or targeted therapy) without losing valuable and characteristic biological antitumoral properties, determined *in vitro* and *in vivo* in animal models.

EXPERIMENTAL PROCEDURES

General. All solvents were dried following standard procedures (dichloromethane (CH_2Cl_2): distillation over P_2O_5, acetonitrile (CH_3CN): distillation over CaH_2, THF: distillation over Na°/benzophenone). *N*,*N*-Dimethylformamide (DMF) was purchased from Fisher Scientific and stored over 3 Å molecular sieve. 1,2-Dimethoxyethane (DME) was dried by storage over 3 Å molecular sieve. *N*,*N*-Diisopropylethylamine (DIEA) was distilled over CaH_2. Column chromatography purifications were performed on Geduran 60 silica gel (40−63 μm) from Merck. TLC were carried out on Merck DC Kieselgel 60 F-254 aluminum sheets. Compounds were visualized by one or more of the following methods: (1) illumination with a short wavelength UV lamp (i.e., λ = 254 nm), (2) spray with a 0.2% (w/v) ninhydrin solution in absolute ethanol, and (3) spray with a 3.5% (w/v) phosphomolybdic acid solution in absolute ethanol. The HPLC-gradient grade acetonitrile (CH_3CN) and methanol (CH_3OH) were obtained from VWR. Phosphate buffered saline (PBS, 100 mM phosphate + 150 mM NaCl, pH 7.5) and aq mobile phases for HPLC were prepared using deionized water purified with a Milli-Q system (purified to 18.2 MΩ.cm).

Instruments and methods: Melting points were recorded on a LEICA VMHB Kofler system at atmospheric pressure. Optical rotations were measured by using a Perkin-Elmer 341 polarimeter. Infrared (IR) spectra were recorded with a universal ATR sampling accessory on a Perkin-Elmer FT-IR Spectrum 100 spectrometer. The elemental analyses were carried out with a Flash 2000 Organic Elemental Analyzer (Thermo Scientific). ^1H and ^{13}C NMR spectra (C13APT or C13CPD experiments) and recorded either on a Bruker AC 200 or on a Bruker DPX 300 spectrometer working at 200 and 300 MHz, respectively. Chemical shifts are expressed in parts per million (ppm) from the residual nondeuterated solvent signal $CDCl_3$ (δ_H = 7.26, δ_C = 77.00) or DMSO-d_6 (δ_H = 2.50, δ_C = 39.43).[19] *J* values are in hertz (Hz). Analytical HPLC was performed on a Thermo Scientific Surveyor Plus instrument equipped with a PDA detector. Semipreparative HPLC was performed on a Thermo Scientific SPECTRASYSTEM liquid chromatography system (P4000) equipped with a UV−visible 2000 detector. Low-resolution mass spectra were obtained with a Finnigan LCQ Advantage MAX (ion trap) apparatus equipped with an electrospray (ESI) source. High-resolution mass spectra were recorded on a LCT Premier XE benchtop orthogonal acceleration time-of-flight (oa-TOF) mass spectrometer (Waters Micromass) equipped with an ESI source and in the positive mode. The absorption spectra were recorded on a Varian Cary 50 scan spectrophotometer by using a rectangular quartz cell (Varian, standard cell, Open Top, 10 × 10 mm, 3.5 mL). The emission/excitation spectra were recorded with a Varian Cary Eclipse spectrophotometer after excitation/emission at the suitable wavelength (excitation and emission filters: auto; excitation and excitation and emission slit: 5 nm) with a semimicro quartz fluorescence cell (Hellma, 104F-QS, 10 × 4 mm, 1400 μL). All fluorescence spectra were corrected. The following equation was used to determine the relative fluorescence quantum yield:[20]

$$\Phi F(X) = (A_S/A_X)(F_X/F_S)(n_X/n_S)^2 \Phi F(S)$$

where *A* is the absorbance at the excitation wavelength. (in the range 0.01−0.1 A.U.), *F* is the area under the corrected emission curve, *n* is the refractive index of the solvents (at 25 °C) used in measurements, and the subscripts S and X represent standard and unknown, respectively. The following standards were used: 7-hydroxycoumarin in PBS (ΦF = 76%) and fluorescein in aq. 0.1 M NaOH (ΦF = 90%).

RP-HPLC separations: The following system was used for the analytical experiments: column Thermo Hypersil GOLD C_{18} (5 μm, 4.6 × 150 mm) with CH_3CN and aq. 0.1% trifluoroacetic acid (aq. TFA 0.1%, pH 2.0) as eluents [100% TFA (1 min), then linear gradient from 0% to 80% (45 min) of CH_3CN]. UV detection at 254 nm. The following chromatographic system was used for the purification step: column Varian Kromasil C_{18} (10 μm, 21.2 × 250 mm) with CH_3CN and aq. TFA 0.1% as eluents with the following gradient [100% TFA (5 min), then linear gradient from 20% to 100% (49 min) of CH_3CN] at a flow rate of 20.0 mL/min. Double UV−vis detection was achieved at 368 and 456 nm.

Pyridone (3). This compound was prepared in 96% e.e. according to the Fang modification[21] of Comins'strategy. The e.e. was determined using HPLC equipped with an analytical column Chiralcel ODH as chiral stationary phase: eluent system: heptane/isopropanol 9/1; flow: 1 mL/min; UV detection: 254 nm; retention times: t_{R1} = 17.94 min (area 1 = 1.95) and t_{R2} = 22.86 min (area 2 = 98.05).

2-Chloro-6-hydroxyquinolin-3-carbaldehyde (5). To a stirred solution of 2-chloro-6-methoxyquinolin-3-carbaldehyde (500 mg, 2.26 mmol) in dry CH_2Cl_2 (15 mL) cooled at −78 °C was added BBr_3 (0.75 mL, 7.91 mmol, 3.5 equiv) dropwise. After stirring for 30 min at −78 °C, the mixture was warmed to rt and stirred for further 2 h. Thereafter, the reaction mixture was cooled to 0 °C and quenched by adding ice and cold deionized water. The resulting mixture was extracted with ethyl acetate (2 × 50 mL). The combined organic layers were washed with brine, dried over anhydrous $MgSO_4$, and concentrated under reduced pressure. The resulting residue was triturated with CH_2Cl_2 to afford a yellow solid (380 mg, 1.83 mmol, yield 82%). Mp 210 °C (decomposition). IR 3278, 1693, 1579, 1500, 1219 cm^{-1}. ^1H NMR (300 MHz, DMSO-d_6) δ 10.50 (s, 1H, OH), 10.35 (s, 1H), 8.79 (s, 1H), 7.90 (d, *J* = 9.0 Hz, 1H), 7.52 (dd, *J* = 2.4, 9.0 Hz, 1H), 7.43 (d, *J* = 2.4 Hz, 1H). ^{13}C NMR (75.5 MHz, DMSO-d_6) δ 189.4, 156.7, 145.3, 143.6, 139.3, 129.2, 127.7, 126.0, 125.9, 110.2. HPLC t_R = 16.1 min, purity >96%. MS(ESI+): *m*/*z* (%): 208 (100) $[M + H]^+$, calcd for $C_{10}H_6ClNO_2$: 208.

6-(2-Azidoethoxy)-2-chloro-quinolin-3-carbaldehyde (6). To a stirred solution of **5** (100 mg, 0.48 mmol) in dried DMF

dx.doi.org/10.1021/bc3005304 | *Bioconjugate Chem.* 2013, 24, 1119−1133

(1.5 mL), under atmosphere of argon, at rt was added anhydrous solid K_2CO_3 (333 mg, 2.4 mmol, 5 equiv). The reaction mixture turned red immediately. After 5 min stirring at room temperature, the the 2-azidoethyl tosylate[27] (126 mg, 0.60 mmol, 1.25 equiv) was added to the solution. The reaction mixture was heated at 50 °C for 12 h. The mixture was cooled to room temperature, solubilized in a minimum of water/DMSO (1:1), and directly filtered over silica gel (EtOAc/cyclohexane 1:1) to afford the 2-azidoethyl ether **6** (143 mg, 0.52 mmol, 63%) as a yellow solid. Mp: 124−126 °C. IR 2928, 2118, 1690, 1577, 1497, 1236 cm^{-1}. ^1H NMR (200 MHz, DMSO-d_6) δ 10.33 (s, 1H), 8.74 (s, 1H), 7.91 (d, J = 9.0 Hz, 1H), 7.65 (d, J = 2.6, 1H), 7.57 (dd, J = 2.6, 9.0, 1H), 4.30 (t, J = 4.6 Hz, 2H), 3.76 (t, J = 4.6 Hz, 2H). ^{13}C NMR (50 MHz, DMSO-d_6) δ 189.3, 156.7, 146.5, 144.5, 139.5, 129.2, 127.4, 126.2, 125.9, 108.5, 67.2, 49.2. HPLC: t_R = 24.9 min, purity >92%. MS(ESI+): m/z (%): 277 (100) $[M + H]^+$, calcd for $C_{12}H_{10}ClN_4O_2$: 277. Elemental analysis (%) calcd: C, 52.09; H, 3.28; N, 20.25; found: C, 52.18; H, 3.27; N, 20.24.

(6-(2-Azidoethoxy)-2-chloroquinolin-3-yl)methanol (7). To a stirred solution of **6** (164 mg, 0.59 mmol) in 4 mL of CH_3OH/CH_2Cl_2 (1:1) at 0 °C was added solid $NaBH_4$ (22 mg, 0.59 mmol, 1 equiv). The reaction mixture was warmed to rt and stirred for 3 h. Then the solution was quenched with a solution of sat. aq. NH_4Cl (20 mL) and extracted with EtOAc (3 × 40 mL). The combined organic layers were washed with brine (20 mL), dried over anhydrous $MgSO_4$, and filtered, and the solvent was removed under reduced pressure. The resulting residue was dissolved in a minimum of DMSO and purified by chromatography over silica gel (CH_2Cl_2 then cyclohexane/EtOAc 1:1) to afford the alcohol **7** (123 mg, 0.44 mmol, 74%) as a yellow solid. Mp: 150−152 °C. IR 3383, 2928, 2107, 1621, 1497, 1221 cm^{-1}. ^1H NMR (300 MHz, DMSO-d_6) δ 8.31 (s, 1H), 7.83 (d, J = 9.0 Hz, 1H), 7.48 (s, 1H), 7.37 (d, J = 9,0, 1H), 5.72 (s, 1H), 4.66 (s, 2H), 4.29 (s, 2H), 3.74 (s, 2H). ^{13}C NMR (75.5 MHz, DMSO-d_6) δ 156.3, 145.8, 141.8, 134.6, 134.0, 129.0, 128.2, 122.1, 106.8, 67.0, 59.8, 49.4. HPLC: t_R = 20.9 min, purity >93%. MS(ESI+): m/z (%): 279.13 (100) $[M + H]^+$, calcd for $C_{12}H_{12}ClN_4O_2$: 279. Elemental analysis (%) calcd: C, 51.72; H, 3.98; N, 20.10; found: C, 51.55; H, 4.07; N, 19.70.

6-(2-Azidoethoxy)-3-(bromomethyl)-2-chloroquinoline (2). To a stirred solution of **7** (121 mg, 0.44 mmol) in dry CH_2Cl_2 (4 mL) cooled at 0 °C was added PBr_3 (45 μL, 0.47 mmol, 1.1 equiv). The reaction was stirred for 12 h at rt. Next, the solution was cooled to 0 °C and quenched by sequential addition of CH_3OH (200 μL) and sat. aq. $NaHCO_3$ (20 mL), extracted with dichloromethane (3 × 30 mL). The combined organic layers were washed with brine (10 mL), dried over anhydrous $MgSO_4$, filtered, and the solvent was removed under reduced pressure. The resulting residue was purified by chromatography over silica gel (cyclohexane/EtOAc 9:1) to afford **2** (97 mg, 0.28 mmol, 65% yield) as a white solid. IR 2931, 2107, 1621, 1494, 1234, 829 cm^{-1}. ^1H NMR (300 MHz, $CDCl_3$) δ 8.08 (s, 1H), 7.89 (d, J = 9.0, 1H), 7.39 (dd, J = 2.1, 9.0 Hz, 1H), 7.03 (d, J = 2.1 Hz, 1H), 4.67 (s, 2H), 4.23 (t, J = 4.8 Hz, 2H), 3.67 (t, J = 4.8 Hz, 2H). ^{13}C NMR (75.5 MHz, $CDCl_3$) δ 156.9, 147.5, 143.4, 137.9, 129.8, 129.7, 128.0, 123.5, 105.8, 67.2, 49.8, 29.8. HPLC: t_R = 29.7 min, purity >98%. HRMS (ESI+): Calc. for $C_{12}H_{11}BrClN_4O$: 342.9784; found: 342.9784.

(*S*)-7-(6-(2-Azidoethoxy)-2-chloroquinolin-3-methyl)-4-ethyl-4-hydroxy-1,7-dihydro-4*H*-pyranol[3,4-*c*]-pyridine-3,8-dione (8). To a stirred solution of **3** (54 mg, 0.26 mmol) in dry DME (4 mL) at 0 °C was added anhydrous *t*BuOK (32 mg, 0.28 mmol, 1.1 equiv). The resulting mixture was stirred at 0 °C for 15 min and at rt for further 15 min. A solution of the benzyl bromide **2** (97 mg, 0.28 mmol, 1.1 equiv) in dry DME (2 mL) was added to the previous solution, and the resulting reaction mixture was stirred for 12 h at rt and 1 h under reflux (for a complete conversion). Thereafter, the mixture was cooled to rt and concentrated. The residue was filtered over a silica gel pad (cyclohexane/EtOAc 1:1 then EtOAc) to afford **8** (73 mg, 0.15 mmol, 60%) as a white solid; Mp: 82−84 °C. IR 3371, 2940, 2109, 1743, 1657, 1599, 1228 cm^{-1}.^1H NMR (300 MHz, $CDCl_3$) δ 7.98 (s, 1H), 7.89 (d, J = 9.0 Hz, 1H), 7.62 (d, J = 7.2 Hz, 1H), 7.40 (dd, J = 9.3; 2.4, 1H), 7.05 (d, J = 2.4, 1H), 6.58 (d, J = 7.2, 1H), 5.57 (d, J = 16.2, 1H), 5.45 (d, J = 15.3 Hz, 1H), 5.24 (d, J = 15.3 Hz, 1H), 5.16 (d, J = 16.2 Hz, 1H), 4.22 (t, J = 4.8, 2H), 3.78 (s, 1H), 3.66 (t, J = 5.1 Hz, 2H), 1.83−1.76 (m, 2H), 0.97 (t, J = 7.2 Hz, 3H). ^{13}C NMR (75.5 MHz, $CDCl_3$) δ 173.6, 158.7, 156.9, 149.0, 146.9, 143.3, 138.2, 138.0, 129.7, 127.9, 127.1, 123.8, 119.1, 105.9, 103.2, 72.1, 67.2, 66.3, 50.4, 49.8, 31.3, 7.6. HPLC: t_R = 23.3 min, purity >86%. $[\alpha]^{22}_D$ +27° (c 2.7, $CHCl_3$). HRMS (ESI+): Calc. for $C_{22}H_{21}ClN_5O_5$: 470.1231; found: 470.1237.

(*S*)-7-(6-(2-*tert*-Butyl ethoxycarbamate)-2-chloroquinolin-3-methyl)-4-ethyl-4-hydroxy-1,7-dihydro-4*H*-pyranol[3,4-*c*]pyridine-3,8-dione (9). The azide derivative **8** (26 mg, 0.05 mmol) was dissolved in a mixture of EtOAc-CH_3OH (2:1, v/v, 3 mL). Di-*tert*-butyl dicarbonate (24 mg, 0.11 mmol, 2 equiv) and Lindlar catalyst (7 mg, 5% by wt) were sequentially added. The reaction flask was purged and flushed with Ar gas then with H_2 gas. The resulting reaction mixture was stirred at rt under an H_2 atmosphere for 12 h. Thereafter, the reaction mixture was filtered through a Celite 545 pad, the filter cake was washed with EtOAc (5 mL), and the combined filtrates were concentrated under reduced pressure. The resulting residue was filtered on silica gel pad by using a step gradient of EtOAc (20−80%) in cyclohexane as the mobile phase affording **9** as a white solid (28 mg, 0.05 mmol, yield 93%); Mp: 88−90 °C. IR 3347, 2977, 1746, 1703, 1658, 1497, 1164 cm^{-1}.^1H NMR (200 MHz, $CDCl_3$) δ 7.95 (s, 1H), 7.86 (d, J = 9.2 Hz, 1H), 7.61 (d, J = 7.2 Hz, 1H), 7.34 (dd, J = 2.4, 9.2 Hz, 1H), 7.02 (d, J = 2.4 Hz, 1H), 6.59 (d, J = 7.2 Hz, 1H), 5.58 (d, J = 16.1 Hz, 1H), 5.42 (d, J = 15.2 Hz, 1H), 5.24 (d, J = 15.6 Hz, 1H), 5.15 (d, J = 16.6 Hz, 1H), 5.07−5.02 (m, 1H), 4.09 (t, J = 5.2 Hz, 2H), 3.79 (s, 1H), 3.56 (t, J = 5.2 Hz, 2H), 1.86−1.75 (m, 2H), 1.43 (s, 9H), 0.97 (t, J = 7.4 Hz, 3H). ^{13}C NMR (50 MHz, $CDCl_3$) δ 173.6, 158.7, 157.3, 155.7, 149.1, 146.7, 143.2, 138.1, 138.0, 129.6, 128.0, 127.1, 123.7, 119.2, 105.9, 103.2, 79.6, 72.1, 67.5, 66.3, 50.3, 39.8, 31.4, 28.3, 7.6. HPLC: t_R = 24.7 min, purity >96%. $[\alpha]^{22}_D$ +27° (c 2, $CHCl_3$). HRMS (ESI+): Calc. for $C_{27}H_{31}ClN_3O_7$: 544.1851; found: 544.1857.

10-(2-*tert*-Butyl ethoxycarbamate)-(*S*)-camptothecin (10). In an oven-dried reaction glass tube, a solution of **9** (18 mg, 0.03 mmol) in dry CH_3CN (1 mL) and KOAc (8 mg, 0.08 mmol, 2.5 equiv) was mixed. Ar gas was bubbled through the reaction mixture for 15 min. Then, $(PPh_3)_2Pd(OAc)_2$ (4.9 mg, 0.006 mmol, 0.2 equiv) was added and Ar gas was bubbled again through the reaction mixture for further 15 min. The flask was sealed and the reaction mixture was stirred at 100 °C for 18 h. Thereafter, the mixture was allowed to cool at rt and then directly filtered over a silica gel pad by using a step gradient of EtOAc (50−100%) in cyclohexane as the mobile phase to afford the desired fused pentacyclic alkaloid derivative **10** as a yellow light solid (12 mg, 0.02 mmol, yield 71%). IR 3345, 2977, 1755, 1656, 1502, 1238 cm^{-1}. ^1H NMR (300 MHz, $CDCl_3$) δ 8.19 (s, 1H),

dx.doi.org/10.1021/bc3005304 | *Bioconjugate Chem.* 2013, 24, 1119−1133

8.04 (d, J = 9.3, 1H), 7.61 (s, 1H), 7.36 (dd, J = 2.1, 9.3 Hz, 1H), 7.06 (d, J = 2.1 Hz, 1H), 5.71 (d, J = 16.2 Hz, 1H), 5.29−5.20 (m, 4H), 4.22 (s, 1H), 4.16 (t, J = 4.8 Hz, 2H), 3.66−3.62 (m, 2H), 1.94−1.83 (m, 2H), 1.47 (s, 9H), 1.01 (t, J = 7.2 Hz, 3H). ^{13}C NMR (75.5 MHz, $CDCl_3$) δ 173.8, 157.6, 157.5, 155.9, 150.1, 149.9, 146.3, 144.7, 131.0, 129.5, 129.2, 129.0, 123.3, 118.0, 106.0, 97.4, 79.7, 72.7, 67.5, 66.1, 50.0, 39.9, 31.4, 28.3, 7.8. HPLC: t_R = 23.5 min, purity >93%. HRMS (ESI+): Calc. for $C_{27}H_{31}ClN_3O_7$: 508.2084; found: 508.2090.

Fluorescein-Isonipecotic Acid Derivative (4). This fluorophore carboxylic acid was prepared according to a procedure recently reported by us.[22]

Fluorescein-Labeled Camptothecin (1). *(a). Removal of the Boc Group.* To a solution of **10** (12 mg, 0.02 mmol) in CH_2Cl_2 (1 mL) cooled at 0 °C was added TFA (0.4 mL, 2.4 mmol, 118 equiv) dropwise and the resulting mixture was stirred at rt for 2 h. Thereafter, the reaction mixture was concentrated, and the residue was triturated with precooled Et_2O to afford the corresponding TFA salt of amino-camptothecin derivative **11**. MS (ESI+): m/z (%): 408 (100) $[M+H]^+$, calcd for $C_{22}H_{22}N_3O_5$: 408.

(b). Amide Coupling Reaction. The TFA salt was dissolved in dry DMF (0.6 mL) and the mixture was cooled to 0 °C. Fluorescein carboxylic acid **4** (12.2 mg, 0.03 mmol, 1.2 equiv), DIEA (20 μL, 0.16 mmol, 7 equiv), HOBt monohydrate (3.6 mg, 0.03 mmol, 1.2 equiv), and DCC (6 mg, 0.03 mmol, 1.2 equiv) were sequentially added. The resulting reaction mixture was stirred at rt for 12 h and then evaporated almost to dryness. The resulting residue was purified by semipreparative RP-HPLC (t_R = 26.91−29.76 min). The product-containing fractions were lyophilized to afford the desired fluorescent bioconjugate **1** as an orange amorphous powder (7.7 mg, 0.01 mmol, overall yield 40% for the two steps). IR 3353, 2940, 1748, 1594, 1453, 1173 cm^{-1}. ^{1}H NMR (300 MHz, DMSO-d_6) δ 8.50 (s, 1H), 8.10−8.04 (m, 2H), 7.70−7.68 (m, 2H), 7.62−7.60 (m, 1H), 7.52−7.46 (m, 3H), 7.27 (s, 1H), 7.14−7.11 (m, 2H), 6.78−6.76 (m, 3H), 5.41 (s, 2H), 5.24 (s, 2H), 4.16−4.12 (m, 2H), 4.05−4.02 (m, 1H), 3.52−3.44 (m, 1H), 3.50−3.45 (m, 2H), 2.36−2.26 (m, 2H), 1.86−1.84 (m, 2H), 1.60−1.56 (m, 2H), 1.22−1.15 (m, 3H), 0.88 (t, J = 6.9 Hz, 3H). ^{13}C NMR (75.5 MHz, DMSO-d_6) δ 173.9, 172.4, 166.3, 157.2, 156.7, 156.6, 150.1, 149.9, 145.6, 143.9, 135.8, 131.6, 130.5, 130.4, 130.2, 130.1, 129.9, 129.6, 129.3, 129.3, 127.1, 123.0, 120.8, 118.3, 115.2, 106.9, 102.8, 96.0, 72.3, 66.8, 65.2, 50.1, 45.6, 41.0, 37.9, 30.2, 28.4, 27.9, 8.5, 7.7. HPLC: t_R = 21.2 min, purity >95%. HRMS (ESI+): Calc. for $C_{48}H_{41}N_4O_{10}$: 833.2823; found: 833.2844.

Compounds, Cell Lines, and Culture Conditions. NIH3T3 mouse fibroblasts cells (obtained from America Type Culture Collection) were cultured in high glucose DMEM supplemented with 10% fetal calf serum (FBS), 2 mM L-glutamine, and 100 U/mL penicillin/streptomycin at 37 °C in a humidified 5% CO_2 incubator. Human cell lines from glioblastoma U87 and T98 were obtained from the American Type Culture Collection. The T98 cells were maintained in HAM-F12 and U87 cells were maintained in DMEM (Invitrogen, Cergy Pontoise, France) containing 10% FBS and 1% sodium pyruvate at 37 °C in a humidified atmosphere containing 5% CO_2. Culture media were replaced every three days.

Topoisomerase I Relaxation Assay. Topo I inhibitory activity of CPT-FI versus CPT was assayed by supercoiled DNA relaxation assay. Supercoiled DNA (TopoGEN, FL, USA) was incubated at 37 °C for 30 min with purified human Topo I (TopoGEN, FL, USA) which was premixed with increasing concentrations CPT-FI (50−200 μM) or CPT (as control, 50 μM to 1 mM), then terminated with proteinase K/SDS stop buffer, and loaded on to 2% agarose gel. The standard reaction system contained: 0.25 μg DNA, 10 mM Tris-HCl, pH 7.9, 1 mM EDTA, 150 mM NaCl, 0.1% bovine serum albumin, 0.1 mM spermidine, and 1 U Topo I extracted from T98 cell lines. The samples were electrophoresed in a horizontal 2% agarose gel in TAE (tris base, acetic acid and EDTA) buffer at 1.5 V/cm during 2 h at room temperature. DMSO concentrations in each reaction were maintained at 1% by the addition of serially diluted drug stocks so as not to produce solvent mediated inhibition of Topo I activity. The gels were only poststained with ethidium bromide, destained in water, and photographed under UV illumination.

Cell Growth Assay. T98 cells were plated in quadruplicates in 12-well plates (Costar, 15 × 10^3 cells/well for 24 h before treatment in HAM-F12 (for T98 cells) and DMEM (for U87 cells), supplemented with 10% FBS. Cells were then incubated in the absence or presence of graded concentrations of CPT (TCI, Zwijndrecht, Belgium) or CPT-FI (0.05 to 5 μM) for 24, 48, and 72 h, respectively. Controls were determined by using a DMSO or FI concentration corresponding to the dilution of CPT used for 5 μM concentration tested. After treatment, cells were harvested, rinsed by PBS, detached by accutase (Millipore, Molsheim, France), and cellular density was measured by direct cell counting in tampon Z-tri-Pak (Beckman, Lognes, France) with an electronic cell counter (Z2, Coulter Beckmann).

Cell Cycle Analysis. T98 cell lines were plated in 75 cm^2 flasks (Techno plastic products AG, Trasadingen, Switzerland). When cells reached 80% confluence, they were incubated in the absence or presence of CPT and CPT-FI (50 nM and 0.5 μM) for 24 or 48 h. Cells treated with DMSO corresponding to CPT concentrations were used as control. Cell cycle analysis was done by DNA staining with propidium iodide by flow cytometry. Briefly, after treatment, cells were trypsinized, harvested in PBS, and fixed in ice cold 70% ethanol for 2 h. Staining was done with 0.6 mg/mL RNase (30 min, RT, Sigma-Aldrich) and 50 μg/mL propidium iodide (30 min, RT, Sigma-Aldrich). Cell cycle status was quantified by FacsCalibur flow cytometer (BD Biosciences) using CellQuest analysis software (Becton Dickinson Immunocytometry Systems) using an excitation laser set at 480 nm and a detection wavelength of 670 nm (FL3), to avoid detection of FI excitation.

Imaging of Camptothecin-FI Incorporation in Living Cells. Glioblastoma T98 cell line cultured in 35-mm glass bottom microwell dishes (MatTek, Ashland, USA) containing growth medium, and maintained in a live cell chamber at a fixed temperature of 37 °C. T98 cellular uptake of CPT and CPT-FI **1** (5 μM) was monitored using a confocal laser-scanning microscope TSC SP5 by video time-lapse microscopy at the gain and offset (Leica, Heidelberg, Germany) equipped with a AOBS system and a white laser (excitation flexibility).

The cellular uptake of CPT and CPT-FI was also examined by flow cytometry. T98 cells were plated in 75 cm^2 culture flasks containing the growth medium 24 h before treatments with CPT and CPT-FI during 5, 15, and 30 min or 24 and 48 h treatments with CPT and CPT-FI (0.5 μM each). The quantitative fluorescence was observed with a FacsCalibur flow cytometer (BD Biosciences) using CellQuest analysis software (Becton Dickinson Immunocytometry Systems) using an excitation laser set at 480 nm and a detection wavelength of 515 nm, to allow detection of FI excitation.

Heterotopic Tumoral Growth Study. Swiss nude mice (Charles River Laboratory, L'Arbresle, France) were kept in a temperature-controlled room (21 ± 1 °C), under an established photoperiod (lights on 07.00−19.00 h) with free access to food and tap water. The work described in this article was carried out in accordance with the Directive 2010/63/EU of the european parliament and of the council of 22nd September 2010 on the protection of animals used for scientific purposes, published in the Official Journal of the European Union L276/33 (20.10.2010) and authorized by the French Ethical Committee. These experiments were conducted under the supervision of authorized investigators (H. Castel; authorization no. 76.98 from the Ministry of Food, Agriculture and Fisheries.

For intratumoral experiments, the tumorigenic NIH3T3 cell lines were used to monitor the direct intratumoral penetration of the CPT-FI. Thus, a cohort of 6- to 7-week-old male Swiss Nude mice (Charles River Laboratory, L'Arbresle, France) was sedated by isoflurane inhalation (Aerane, Baxter) and implanted subcutaneously (s.c.) into right flanks with 1×10^6 NIH3T3 cells/100 μL PBS. A stock solution of CPT-FI in DMSO (10^{-2} M) was prepared and stored at −20 °C. Aliquots of CPT-FI at 40 mg/kg, were freshly prepared in DMSO/NaCl 0.9%, for each day injection. When tumors reached a volume of 700 mm^3, 10 μL of CPT-FI or vehicle at the corresponding concentration were injected in the tumor. Tumors sizes were measured every two days by the use of a caliper (Bioblock, 0.01 mm precision, Fisher Scientific SAS, Illkirsh, France) and volume was calculated as $V = (1/2)a \times b^2$ (a, length of the apparent tumoral mass; b, width of the apparent tumoral mass). Mouse weight was also controlled every two days. Animals were sacrificed when tumors reached the maximal ethical volume of 2000 mm^3. Tumors were immediately collected, frozen in isopentane, and maintained at −80 °C until immunohistochemistry experiments.

For intravenous administration of FITC or CPT-FI, and tumor distribution, a cohort of 6- to 7-week-old male Swiss Nude mice (Charles River Laboratory, L'Arbresle, France) was sedated by isoflurane inhalation (Aerane, Baxter) and implanted subcutaneously (s.c.) into right flanks with 1×10^6 glioblastoma cell line U87 cells/100 μL PBS. A stock solution of FITC or CPT-FI in DMSO (10^{-2} M) was prepared and stored at −20 °C. Aliquots of CPT-FI were freshly prepared in DMSO/NaCl 0.9% for each injection. When tumors reached a volume of 300 mm^3, 100 μL of FITC (66 mg/kg; 0.5 μmol) or CPT-FI (66 mg/kg) was injected *via* the tail vein. Animals were sacrificed 4 or 8 h after bolus administration of the fluorescent molecules. Tumors were immediately collected, frozen in isopentane, and maintained at −80 °C until immunohistochemical analysis.

Immunohistochemical Staining. NIH3T3 Tumor sections (60 μm thick) or U87 tumor sections (60 μm thick) resulting from intravenous exposure to FITC or CPT-FI, were cut in a Cryostat (Cryostat CM1950, Leica microsystèmes, Nanterre, France), mounted on gelatin-coated slides and maintained at −20 °C until experiment. Briefly, slides were first rinsed in PBS, fixed in a paraformaldehyde (PFA) solution (4%, 20 min, RT), and washed three times in PBS. Sections were permeabilized and preincubated in a PBS, BSA 0.1%, NDS, 1:50, Triton X100 0.3%. Slides were then incubated with 4′,6-diamidino-2-phenylindole dihydrochloride (DAPI, 1/1000^e, 10 min, RT, Sigma-Aldrich, Saint Quentin Fallavier, France), washed again, and mounted in Mowiol 4−88 (Calbiochem, Meudon, France). U87 tumors were co-immunostained with an anti-Collagen IV antibody (Santa Cruz Biotechnology, Le Perray-en-Yvelines, France), in order to visualize hyperplastic tumor vessels. Slices were then examined using a confocal conventional microscope (Leica TCS SP2 AOBS, Nanterre, France) and a macroconfocal miscroscope (Leica TCS LSI). Analyses from the confocal acquisitions were achieved by using the ImageJ 1.44. software.

Statistical Analysis. All statistical analyses were conducted using the GraphPad Prism 4.00 software (GraphPad Software). Among the growth tumoral cell experiments, nonparametric statistical tests were used, i.e., Kruskal−Wallis ANOVA and Mann−Whitney tests for dual comparisons. $P < 0.05$ was considered as significant.

RESULTS AND DISCUSSION

To illustrate the proof-of-concept of possible fluorescent modifications of chemotherapy for investigation of biodistribution and pharmacokinetic, the most classical camptothecinoid, 20(*S*)-camptothecin, was selected as bioactive model compound, along with the well-established fluorescein as the green emitting fluorescent label.[23] Although near-infrared probes are ordinarily used for *in vivo* imaging, green fluorescence dyes have been preferred and widely used to image tumors and superficial tissues

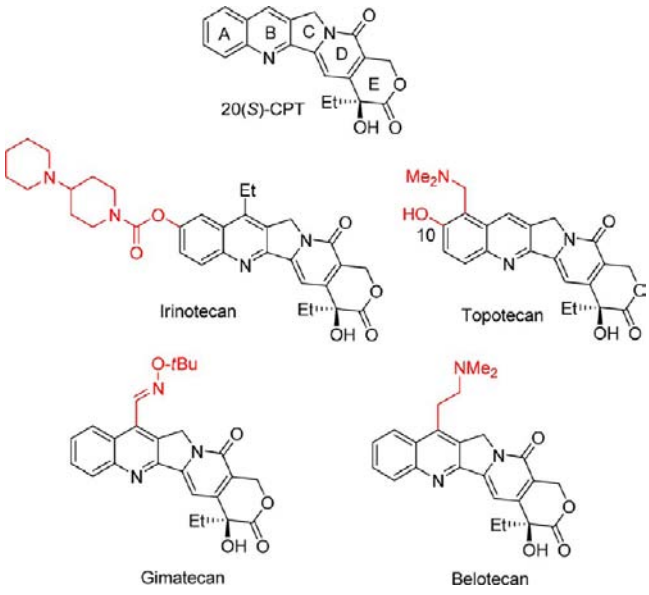

Figure 1. Camptothecin and its derivatives.

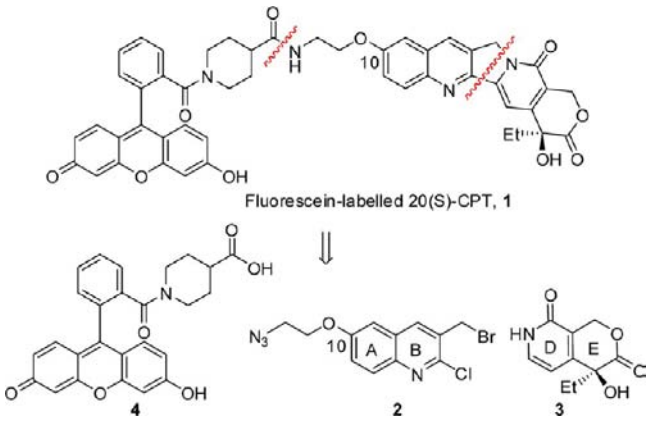

Figure 2. Fluorescein-labeled CPT **1**: retrosynthetic analysis.

dx.doi.org/10.1021/bc3005304 | *Bioconjugate Chem.* 2013, 24, 1119−1133

Scheme 1. Synthesis of AB and CD Ring Systems 2 and 3

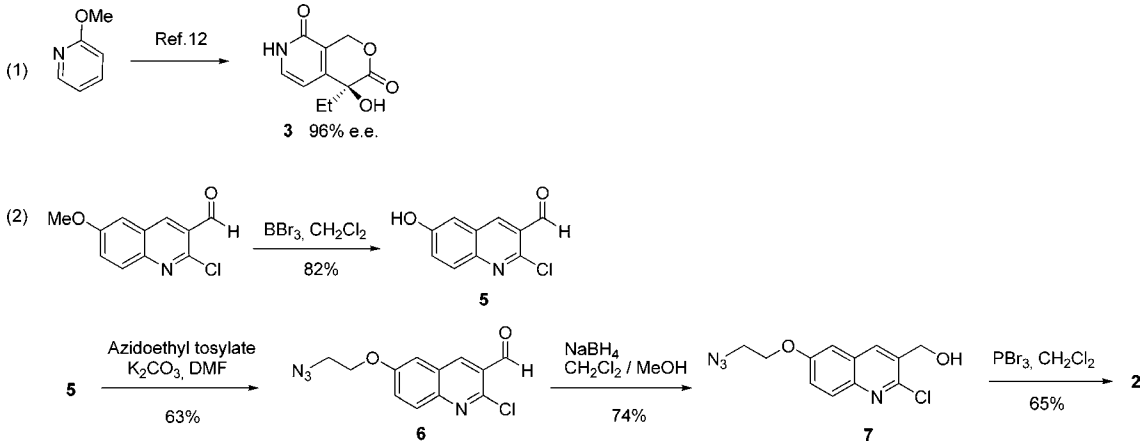

Scheme 2. Synthesis of the Fluorescein-Labeled CPT 1

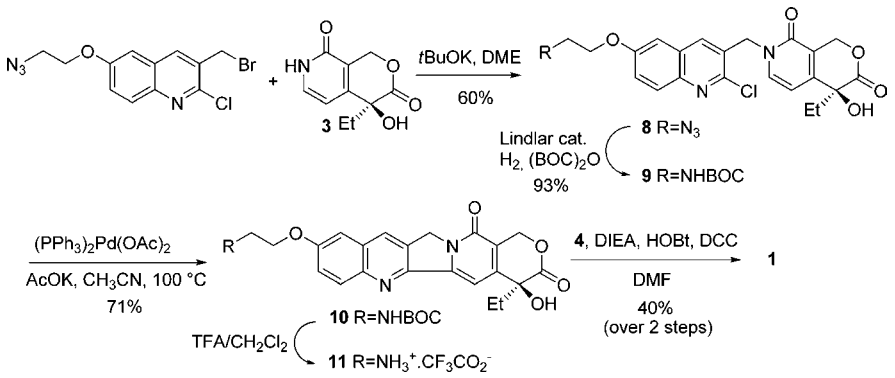

Scheme 3

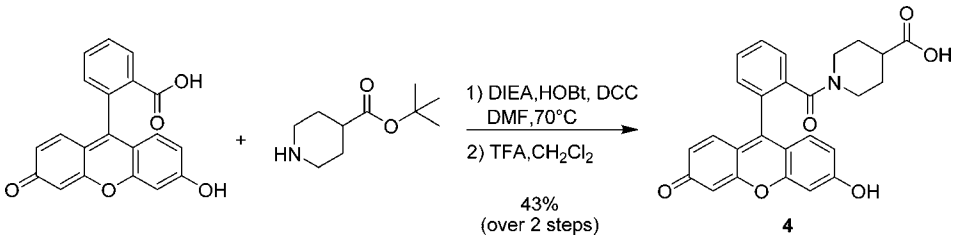

Table 1. Photophysical Properties of Fluorescent Conjugate 1 and of Its Components 11 and 4 in PBS at 25 °C

Cmpd	$\lambda_{abs,\ max}$ (nm)	ε (dm^3 mol^{-1} cm^{-1})	$\lambda_{em,\ max}$ (nm)	Φ_F (%)
CPT-FI **1**	265, 378, 502	21550, 17500, 28835	424, 524	37%[a]
4	499	47700	522	79%[a]
11	265, 363, 378	29250, 27640, 30740	424	61%[b]

[a]For $\lambda_{abs,\ max}$ = 502 and 499 nm, respectively; and determinated by using fluorescein (Φ_F = 90% in aq. 0.1 M NaOH) as standard (excitation at 460 nm). [b]For $\lambda_{abs,\ max}$ = 363 nm; and determinated by using 7-hydroxycoumarin (Φ_F = 76% in PBS) as standard (excitation at 350 nm).

on small animals such as mice, mainly because of the short penetration distance of green light in tissue. [24]

To be viable and rapidly extended to a wide range of CPT analogues used as cancer therapy in patients, a late stage modular synthetic approach to the fluorescent conjugate was investigated. Also, it is noteworthy that most of the biologically active analogues are AB and/or E ring modified CPT. Consequently, the synthetic route chosen for the construction of the fluorescent conjugate involves the sequential and late stage assembly of three distinct molecular units: the AB ring system **2** with DE pyridinone-based heterocycle system **3** (described by Comins)[25] and finally the subsequent peptide-type coupling reaction between the pentacyclic alkaloid formed and the fluorophore **4** (Figure 2). The use of an unusual fluorescein derivative bearing a tertiary amide of isonipecotic acid at the 2′-position instead of the current carboxyl group was preferred to provide steric protection and so to improve the photostability of the fluorescein core.[26] Furthermore, this is the most common way to avoid the undesired cyclization equilibrium leading to the formation of the colorless and nonfluorescent spirolactone (especially at pH < 6). This fluorescein derivative exhibits valuable fluorescence properties in the green spectral region and was attached at the C10 position of the A-ring of the bioactive compound to retain the biological activity. Indeed, substitution on rings C, D, and E is usually not well tolerated,[13] and introduction of an electron-rich

dx.doi.org/10.1021/bc3005304 | Bioconjugate Chem. 2013, 24, 1119−1133

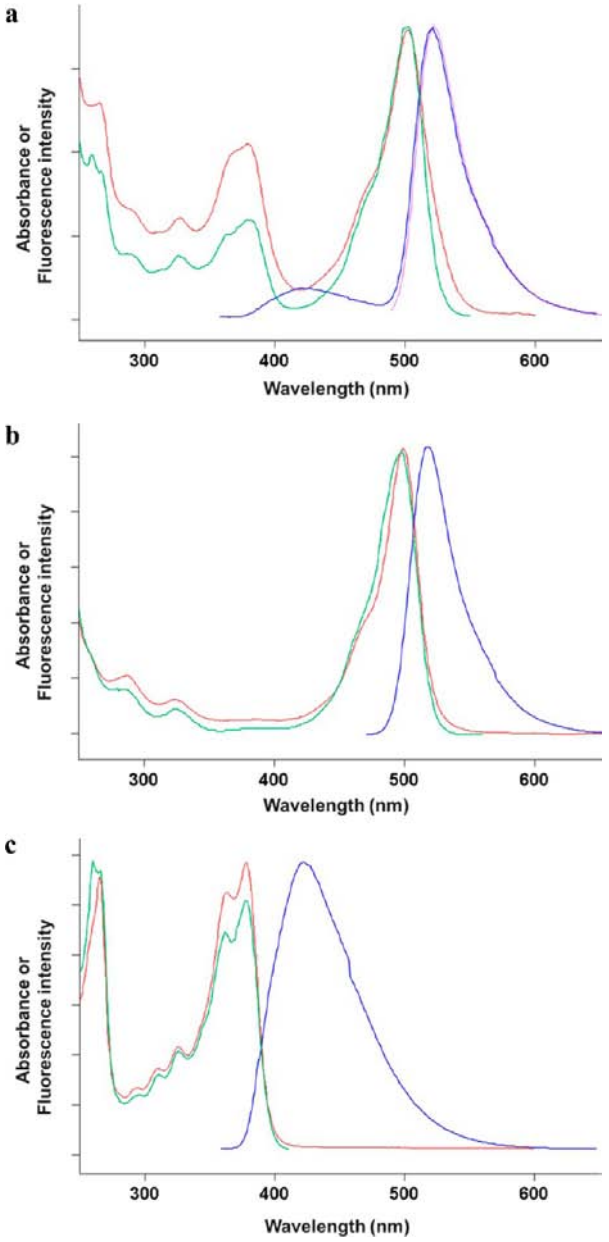

Figure 3. Normalized absorption (red), emission [(blue) λ_{ex} 350 nm and (magenta) λ_{ex} 480 nm for **1**, (blue) λ_{ex} 350 nm for **11** and 460 nm for **4**] spectra, and excitation [(green), λ_{em} 425 nm for **1**, 570 nm for **4**, and 560 nm for **11**] of (a) camptothecin–fluorescein conjugate CPT-FI **1** in PBS at 25 °C; (b) fluorescein-isonipecotic acid derivative **4**; (c) aminated CPT derivative **11**.

function at C10 position does not alter the biological activity of CPT, as illustrated by the C10 phenol substitution found in the topotecan structure (Figure 1).

The DE ring fragment **3** was prepared from 2-methoxypyridine according to the Fang modification of Comins'strategy in 96% e.e. (Scheme 1, part 1).[21] The AB building block **2** was synthesized in four steps from commercially available 2-chloro-6-methoxy-3-quinolinecarboxaldehyde (Scheme 1, part 2). First, deprotection of the aromatic methyl ether was achieved with BBr_3 in dry CH_2Cl_2 to afford **5** in 82% yield. Next, the resulting phenol derivative was reacted with 2-azidoethyl tosylate[27] in a standard S_N2 reaction to give the corresponding ether **6**. It is noteworthy that the azido group has proven to be a particularly useful amine precursor due to its good stability under both acidic and basic conditions required for the next steps of the synthesis. The aldehyde **6** was readily reduced with $NaBH_4$ in CH_2Cl_2–MeOH leading to the corresponding alcohol **7** in a good 74% yield. Final treatment of the primary alcohol with phosphorus tribromide in dry CH_2Cl_2 afforded the AB fragment **2** with 65% yield.

The two fragments **2** and **3** were joined as described, on treatment with *t*-BuOK in 1,2-dimethoxyethane (DME) to provide the tetracycle **8** (Scheme 2). However, the Heck ring-closure strategy failed to form the C ring system, whatever the reaction conditions tested, probably due to the presence of the azido functionality. However, the use of Lindlar catalyst along with $(Boc)_2O$ directly and chemoselectively reduced azido **8** into the corresponding *N*-Boc-protected amine **9** in almost quantitative yield (93%), without dehalogenation of the aromatic chloride.[28] Gratifyingly, the Heck reaction proceeded to afford the corresponding pentacyclic alkaloid **10** in a good 71% yield. Next, the Boc group was removed with trifluoroacetic acid (TFA) in CH_2Cl_2 to furnish the corresponding primary amine **11**. The amine-reactive labeling reagent **4** derived from fluorescein was prepared using an optimized (two-step) procedure inspired by the work of Gao et al. (Scheme 3).[26] Amidification of fluorescein with *tert*-butyl isonipecotate was readily achieved by treatment with DCC-HOBt in dry DMF. Thereafter, the *tert*-butyl ester was removed by TFA in CH_2Cl_2. Due to the high polarity of the resulting carboxylic acid derivative, a purification by semipreparative RP-HPLC was found more convenient than standard chromatography over silica gel. Thus, fluorescein **4** was obtained with a good 43% overall yield. Compared to the synthetic protocol reported by Gao et al.,[26] which involves the chromatographic isolation of the *N*-hydroxysuccinimidyl ester (NHS ester) of fluorescein prior to its aminolysis with an alkyl isonipecotate derivative, our synthetic alternative significantly improved the yield and shortened the overall duration of the synthetic process.[22] Finally, this fluorescent carboxylic acid was coupled to the primary amino group of **11** under standard peptide-coupling conditions. In our case, DCC-HOBt in the presence of DIEA was preferred to a phosphonium or an uronium salt (such as BOP or TSTU) because these latter coupling reagents are prone to react with the phenol group of fluorescein to give undesired side-products leading to a dramatic drop in the isolated yield for the targeted fluorescent compound. The formation of the CPT-fluorescein conjugate **1** (CPT-FI) was carefully checked by analytical RP-HPLC to avoid overcoupling reaction between the product **1** and the unreacted fluorescein **4**. Upon completion of the conjugation reaction, the crude mixture was directly purified by semi-preparative RP-HPLC to isolate pure compound **1** in a satisfying 40% yield over 2 steps. Its structure was confirmed by various spectroscopic data and its high purity was checked by RP-HPLC (see Supporting Information). Analysis of **1** using ESI mass spectrometry indicated the covalent attachment of the fluorescein label and confirmed the integrity of the pentacyclic scaffold of CPT. Thus, the first synthesis of CPT-FI was achieved in 11 steps and 1.4% overall yield from commercial 2-methoxypyridine and 15.8% from the known pyridinone **3**.

With the fluorescent probe **1** in hand, its complete photophysical properties were determined, along with those of **4** and **11** (Table 1 and Figure 3), under simulated physiological conditions (i.e., phosphate buffered saline (PBS), pH 7.5), to ensure that the spectral properties of the fluorescein core were kept upon its conjugation to the CPT alkaloid scaffold. As

dx.doi.org/10.1021/bc3005304 | *Bioconjugate Chem.* 2013, 24, 1119–1133

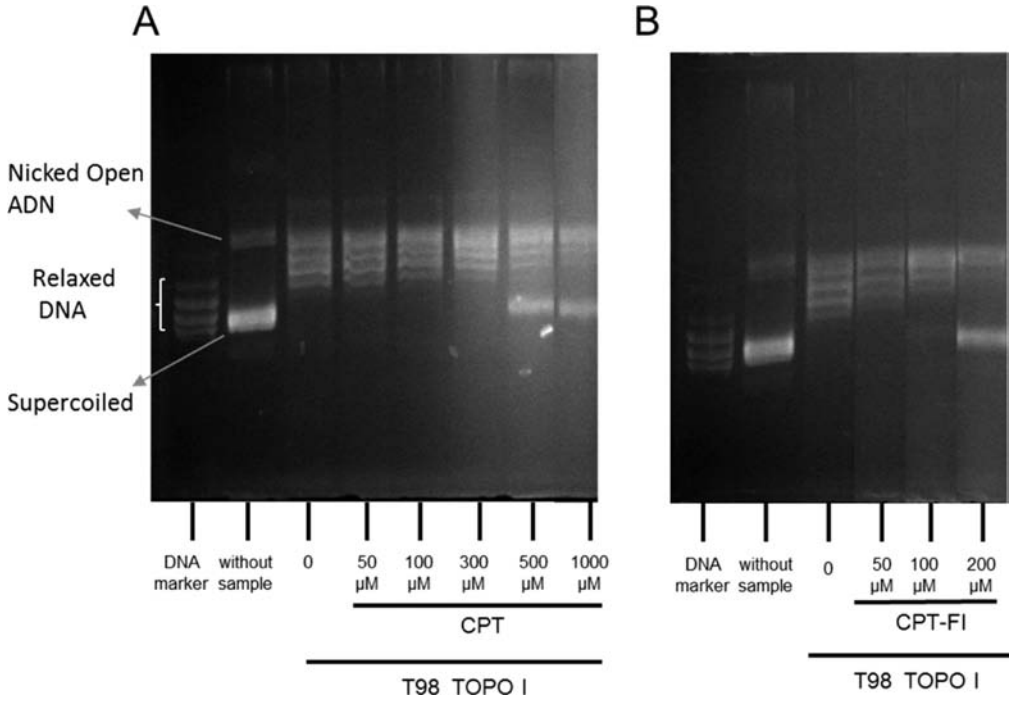

Figure 4. Effect of CPT-FI on the catalytic activity of topoisomerase I extracted from T98 glioblastoma cell nuclei. Supercoiled plasmid DNA was as incubated in the presence of 1 μL nuclear cell lysat from T98 either alone (lanes 3, 0 μM) or with increasing concentrations of camptotecin (CPT, A) at 50 (lane 4), 100 (lane 5), 300 (lane 6), 500 (lane 7), and 1000 μM (lane 8) (A) or CPT-FITC (CPT-FI, B) at 50 (lane 4), 100 (lane 5), and 200 μM (lane 6). Lane 1, relaxed DNA marker; lane 2, supercoiled plasmid DNA with nicked open DNA.

expected, the UV−vis absorption spectrum of the conjugate **1** was the sum of CPT derivative **11** and fluorescein **4** (Figure 3a), which suggests very weak or no electronic interaction (e.g., ground-state dimer) between these two fluorophores in the ground state. Although the fluorescein derivative **1** displays a smaller fluorescence quantum yield of 37% compared to the parent free xanthene dye **4**, satisfyingly, its emission and excitation spectra of **1** are in good agreement with those recorded for **4** or those generally reported for fluorescein derivatives such as **4** (Figure 3b). Consequently, as anticipated and experimentally validated, the fluorescein part of the chromophoric pair **1** could be selectively excited at 480 nm demonstrating attractive spectral factures suitable for further biological imaging applications (Figure 3a). Finally, for informative purpose, the ability of the CPT part of the probe to transfer energy to the fluorescein moiety was also investigated. Indeed, as illustrated in Figure 3a, upon excitation at 350 nm (absorption maximum of CPT core), CPT-FI exhibits a strong green emission band centered at 524 nm and a weak blue emission band at 424 nm, indicating energy transfer between these two FRET partners with efficiency up to 91% (see Supporting Information for details about the energy transfer efficiency (E. T. E.) calculation).

Next, biological properties of the conjugate **1** were investigated and compared with the CPT of interest, 20(*S*)-camptothecin. In order to verify whether CPT-FI exhibited a similar CPT-inhibitory activity on Topoisomerase I (TOPO I) activity, we first extracted nuclear proteins from T98 cells and then evaluated the respective roles of CPT and CPT-FI on TOPO I activity. Then, we showed that T98 nucleus lysates converted a majority of supercoiled DNA into relaxed DNA as observed in lanes 2 and 3 (Figure 4A and B). Increasing concentrations of CPT (50−1000 μM) and CPT-FI (50−200 μM) prevented the supercoiled DNA from being converted into relaxed DNA (Figure 4A and B), CPT-FI being more efficient than CPT in reproducible experiments. Thus, we demonstrate that CPT-FI exhibit a very potent inhibitory control of TOPO I from T98 suggesting that the linker modification of CPT to cross FITC would have even favor CPT affinity for TOPO I.

The prolonged exposure of proliferating and/or tumoral cells to topoisomerase inhibitors as CPT-derivatives results from DNA alteration and apoptotic events.[29−31] Accurate evaluation of the impact of CPT-FI as efficient anti-neoplasic compound, passed first through measurement of drug distribution using *in vitro* model systems, as a more practical method of determining how efficiently a drug penetrate cells. Thus, we first compared the kinetics of incorporation of CPT and CPT-FI in cultured human glioblastoma cell line T98. CPT-FI (0.5 μM) was shown to be rapidly internalized (*short-term*, Figure 5a) in T98 cells after 5 min treatment, and appeared persistently cell-captured from 24 to 48 h (*long-term*, Figure 5b), yielding a 10-fold increase in intracellular intensity value from 5 min to 48 h treatment (Figure 5c). We then performed time-lapse confocal microscopy of CPT-FI (5 μM) incorporation into living T98 cells. When extracellularly applied, the fluorescence was detected after 5 min of exposure, as revealed by punctuate fluorescent dots detected around cell nuclei (Figure 5f). As expected, upon excitation laser set at 480 nm, the autofluorescence of CPT could not be detected either at 5 or 30 min postincubation as shown in Figure 5e (see Supporting Information). Retention in tumor cells can be due to binding at the site of lethal activity (usually DNA), although basic drugs can be sequestered in acidic organelles such as perinuclear endosomes.

We thus hypothesize that specific labeling of CPT with FI may increase fluorescence intensity and/or facilitate detection with microscopic available equipments facilitating the detection by optical imaging.

dx.doi.org/10.1021/bc3005304 | *Bioconjugate Chem.* 2013, 24, 1119−1133

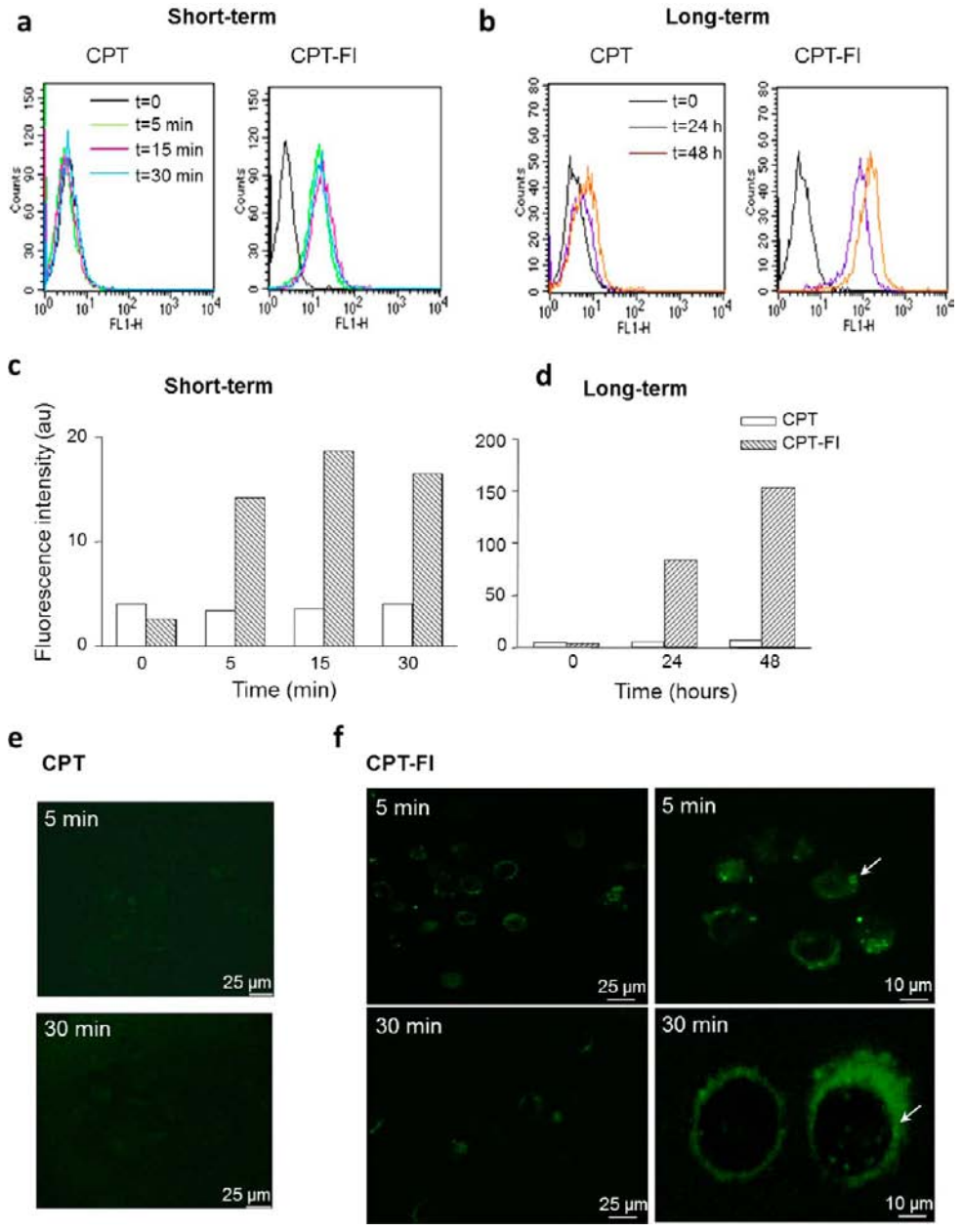

Figure 5. Fluorescent detection of CPT-FI incorporation in glioma cells. (a and b) Flow cytometric analysis of the CPT (0.5 μM) autofluorescence and CPT-FI (0.5 μM) fluorescence within the cytosolic compartment of the glioma cell line T98 at short-term (a) and long-term (b). Fluorescent cells were detected at the laser wavelength of 480 nm in permeabilized conditions. The black lines depict results from control autofluorescence in the absence of CPT, and color lines indicate fluorescence at 5 (green), 15 (red), and 30 min (blue) of treatment (a) or 24 (orange) and 48 h (violet) of treatment (b). (c) Histograms of the mean fluorescence intensities in the cytosol obtained from two representative experiments shown in (a) (short-term) and (b) (long-term) in T98 glioma cells. (d) Confocal autofluorescence control images of CPT (5 μM)-incorporated T98 cells after 5 and 30 min incubation. (e) Confocal fluorescence images of the CPT-FI (5 μM) after 5 and 30 min incubation at low (left) and higher (right) magnification. White arrows indicate drug accumulation around cell nuclei, and green dots are clearly visible in the nucleus.

Then, we compared the impact of CPT and CPT-FI analogues on growth of the glioblastoma U87and T98 human cell lines from 24 to 72 h of treatment. Both cell lines were exposed to increasing concentrations yielding dose-dependent proliferation rate inhibition starting from the 24 h treatment. Phase contrast microphotographs of nontreated T98 glioblastoma cell lines, showed an adherent monolayer of polygonal cells (Figure 6a). In the presence of CPT, and in a lesser extent, CPT-FI, there was a morphological response characterized by cytoplasm retraction and rounding up of the cell body, compared to untreated cells (0) (Figure 6a). These effects were accompanied by a modified glioma cell morphology and integrity, suggestive of a drastic impact of the two CPT analogues on human glioma growth and apoptosis. Moreover, the strong CPT-FI staining observed at 5 μM could be assigned to their aggregation (c.f. Supporting Information for comparative solubility studies between CPT-FI and CPT). As shown in Figure 5b, the dose−response curves indicate that CPT efficiently decreased cell growth from the 0.05 μM concentration. Likewise, CPT-FI showed significant cytotoxic effects on the two cell lines in time- and dose-dependent manners (Figure 6b and c).

dx.doi.org/10.1021/bc3005304 | *Bioconjugate Chem.* 2013, 24, 1119−1133

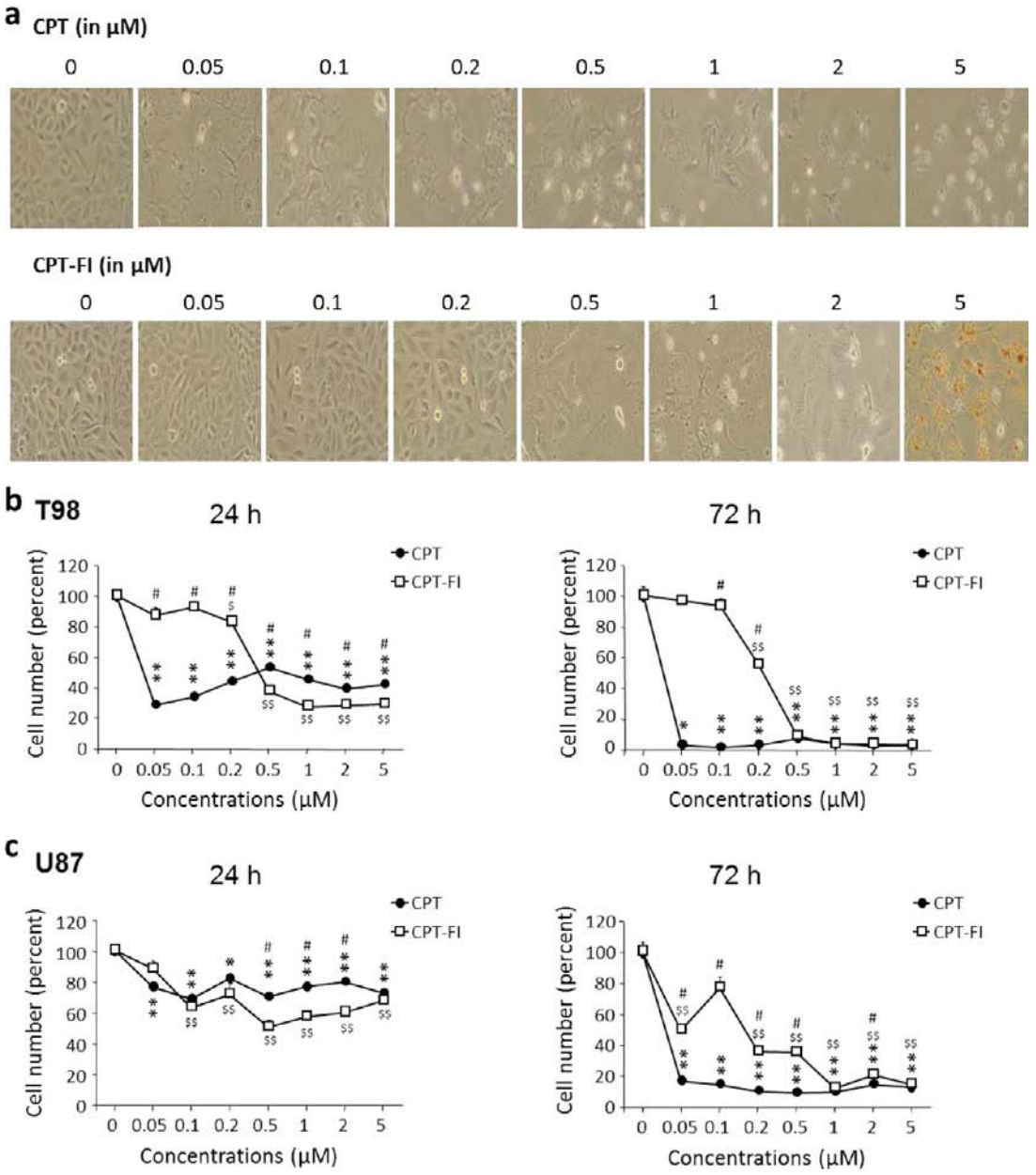

Figure 6. Antiproliferative effect of CPT and CPT-FI on human glioma cells *in vitro*. (a) phase contrast photomicrographs of human glioblastoma cells U87 in the absence (0 μM) or the presence of CPT (top) and CPT-FI (down) from 0.05 to 5 μM each during 24 h. (b and c) T98 (b) or U87 (c) cells were incubated for 24 and 72 h with graded concentrations of CPT or CPT-FI (0.05 to 5 μM) and counted using a Coulter counter. The active and potent camptothecin derivates induce growth inhibition and morphologic changes. Data are mean of a representative experiment in quadruplicate. Statistical significance *, $P < 0.05$; **, $P < 0.01$; CPT groups versus vehicle group (culture medium), \$, $P < 0.05$; \$\$, $P < 0.01$; CPT-FI groups versus vehicle group (culture medium) were determined by Kruskal–Wallis test followed by Mann–Whitney tests *post hoc* test. Statistical significance #, $P < 0.05$; CPT versus CPT-FI groups was determined by Mann–Whitney tests.

CPT and CPT-FI showed cytotoxicity, causing antiproliferating activity in glioma cell lines in a dose- and time-dependent manner. CPT-FI exhibited more than a 10-fold decrease of the CPT efficiency in T98 and retained equivalent activity in U87. These observations show a real interest in use of the CPT-FI for body distribution and understanding of exposed noncancerous organs.

In order to verify whether morphological changes and cell growth inhibition observed after CPT-FI may be associated to topoisomerase and DNA duplication arrest, cell cycle was investigated in T98 in the absence or the presence of both CPT and its derivatives (Figure 7). The cell cycle distribution of the T98 glioblastoma cell line was examined *via* flow cytometry, in the absence or the presence of CPT (0.05 and 0.5 μM) after 24 h treatment, or CPT-FI (0.05 and 0.5 μM) after 24 and 48 h treatment. At 24 h, CPT induced a dose-dependent increase of the G2/M phase from 13% (control) to 24% (0.05 μM) and 73% (0.5 μM), accompanied by a decrease of cell populations in the S phase of the cell cycle, from 17% to 11% (Figure 7a). In contrast, CPT-FI failed to markedly alter cell cycle after 24 h, but evoked a CPT-like G2/M cell accumulation after 48 h treatment (Control, 15%; 0.05 μM, 19%; 0.5 μM, 43%) (Figure 7b). CPT-FI exhibits inferior cytotoxic effect than CPT partly due to its lower solubility in physiological pH. Indeed CPT-FI markedly

dx.doi.org/10.1021/bc3005304 | *Bioconjugate Chem.* 2013, 24, 1119–1133

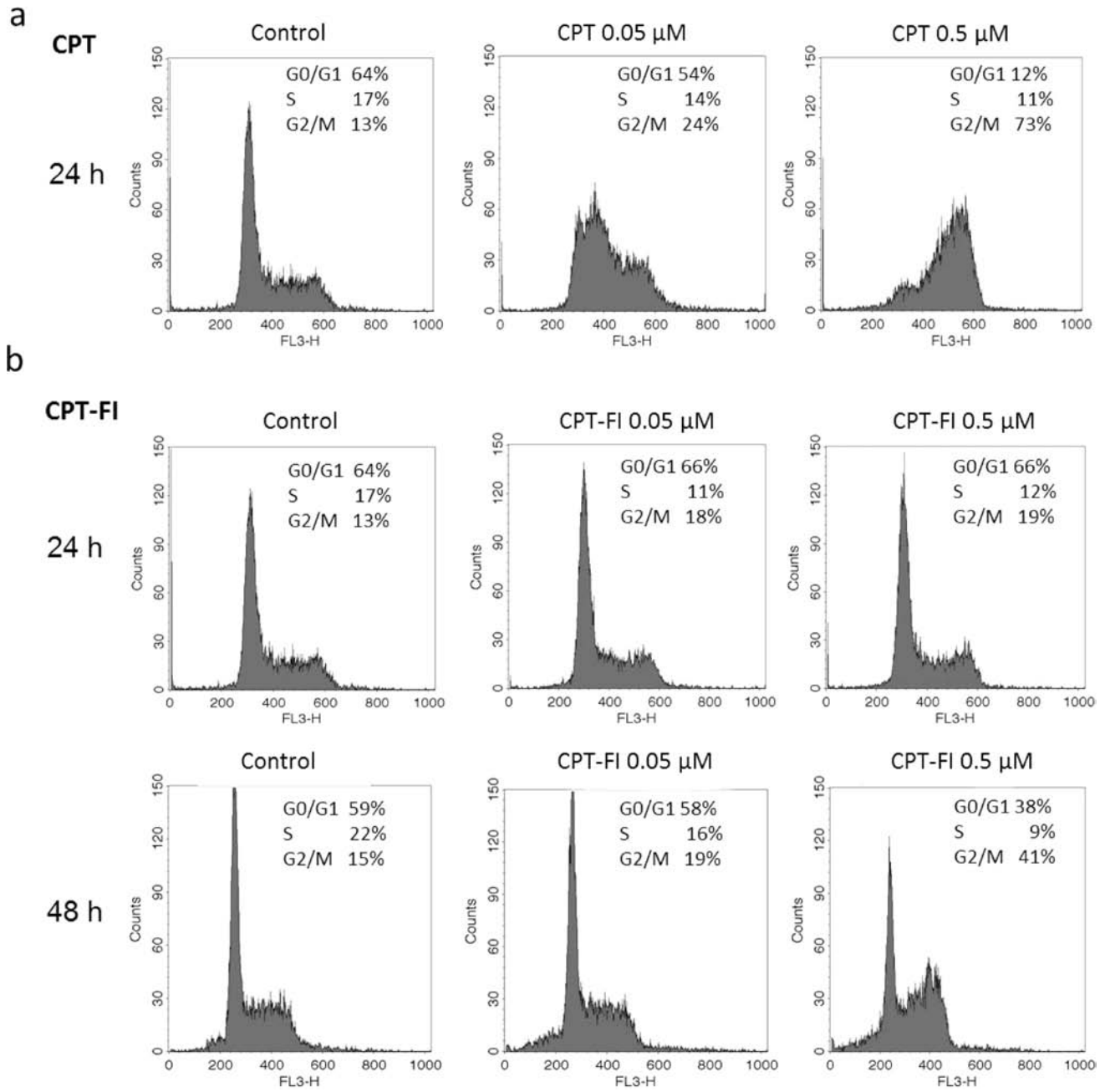

Figure 7. Flow cytometry analysis of glioma cell cycle alteration induced by CPT and CPT-FI in T98. Cells were harvested at 24 h and/or 48 h treatment and analyzed for DNA content by propidium iodide staining in FL3 to avoid contamination by the FI fluorescence. The percentage of T98 cells in the different phases of cell cycle are indicated in each histogram. (a) Cell cycle analysis in the absence or presence of CPT 0.05 and 0.5 μM at 24 h. (b) Cell cycle analysis in the absence or presence of CPT-FI 0.05 and 0.5 μM at 24 and 48 h. Glioma cells showed robust G2 phase arrest after 24 h CPT and 48 h CPT-FI (0.5 μM each). Data refer to one of three performed experiments.

precipitates at 5 μM (40%) while this phenomenon was observed from 10 μM with CPT (c.f. Supporting Information). This observation suggests that we compare the effects of 5 μM CPT with those of 3 μM CPT-FI on cell cycle and toxicity. Besides, it has been reported that substituents at position 10 of the quinoline part of the CPT derivatives may interact with the receptor site with the drug binding site of topoisomerase I cleavage complexes.[32,13] While small substituents at the 10 position of the A ring generally increase efficacy in DNA topoisomerase I inhibition, the presence of bulkier groups should lead to more diminished inhibitory activity. Interestingly, the modification of CPT presented here to bear a bulky fluorescein derivative, displays a better affinity toward topoisomerase I than the native CPT. However, we observed *in cellulo* activity of CPT-FI that was lower than that of the unmodified CPT, likely attributed to lower hydrophobic properties and reduced membrane penetration, to reach the cell nulei. Together these results confirm that CPT induced accumulation in G2/M and T98 glioblastoma cell arrest, and also demonstrate that CPT-FI provokes similar effects but requires longer incubation time and/or higher concentration, establishing the anticancer efficiency *in vitro* of the CPT-FI derivative.

Unfortunately, most drugs are not amenable to direct *in vivo* follow-up because they lack sufficient color or fluorescent

dx.doi.org/10.1021/bc3005304 | *Bioconjugate Chem.* 2013, 24, 1119−1133

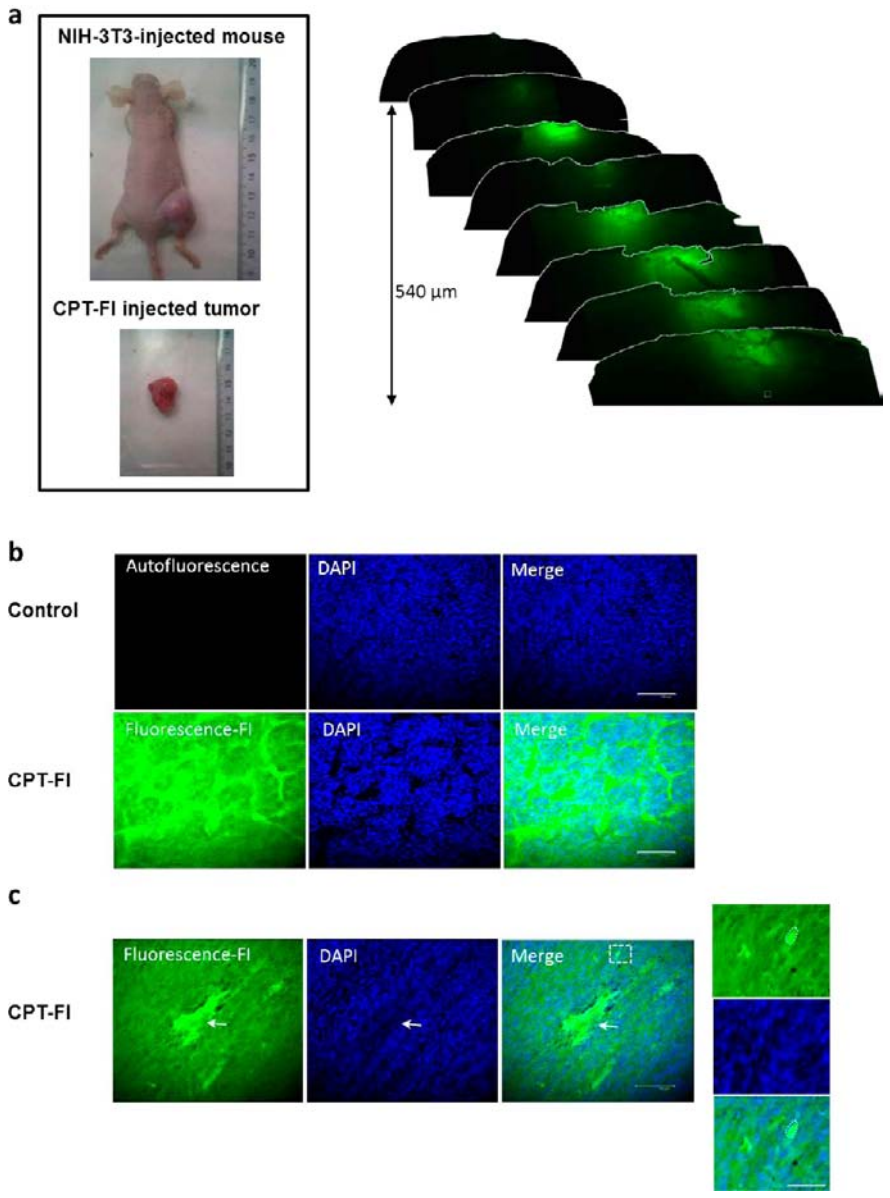

Figure 8. Fluorescent detection of CPT-FI in HIH-3T3-forming tumors in Nude mice. Tumor formation was assessed after subcutaneously inoculating 1×10^6 NIH-3T3 cells into right flanks. Tumors reaching 700 mm^3 were treated *via* intratumoral injections of CPT-FI once a day during 4 days. Four mice were used for this experiment. (a) Photograph of a nude mouse with a solid tumor and enlarged image showing the phenotype of the extracted well delimited tumor before freezing, adjacent to the ruler indicating tumor size in mm (left). Right, alignment of consecutive sections of a CPT-FI treated NIH-3T3 tumor (daily during 4 days), showing green fluorescence around the site of the injection, whereas the rest of the tumor appears less labeled. The white square of the last section indicates the area shown in b with enlarged images. (b) Histological analysis of the tumors derived from NIH-3T3 injected Nude mice. Top, Distribution in tumor sections of the autofluorescence of control tumor (treated with PBS/DMSO) and nuclei counterstained with DAPI (blue). Bottom, Distribution in a tumor section of the CPT-FI fluorescence (green, treated with CPT-FI 40 mg/kg in PBS/DMSO) and nuclei counterstained with DAPI (blue). Scale bars, 125 μm. Merge images correspond to the overlay of the DAPI labeling with control autofluorescence or CPT-FI green fluorescence. (c) Histological analysis of the CPT-FI distribution deeper in the tumor. Left, distribution in a tumor section of the CPT-FI fluorescence (green) and nuclei counterstained with DAPI (blue). The white arrows indicate the strong FI labeling and the less intensely stained nuclei suggesting a preapoptotic zone. Scale bars, 125 μm. Right, Images of digitally zoomed corresponding images of a tumor area (white square) showing that FI labeling colocalizes with DAPI (cell delimitated by the white dotted circle). Scale bar, 60 μm.

properties except the clinically used drugs doxorubicin, mitoxantrone, and topotecan, which exhibit autofluorescence. But initial evidence for limited penetration through tissue of the commonly used anticancer drug doxorubicin was obtained by studying the distribution of its fluorescence in a multicellular layer model.[33] Here, to further extend the possible use of our CPT-fluorescent probe as a cytotoxic drug whose fate can be followed *in vivo*, intratumoral administrations of CPT-FI (CPT-FI, 5 μM, $n = 4$) were performed once daily during four days in xenogafts of NIH-3T3 murine fibroblastic cells in Nude mice (Figure 8a). As compared to intratumoral injections of PBS/DMSO (sham, $n = 4$, *not shown*), histological examination of CPT-FI injected tumors revealed that green fluorescence accumulated to the greatest extent at the border of the tumor and near the site of injection (Figure 8a). At higher magnification, CPT-FI appeared to be mainly distributed in lacks area surrounding apparent viable cells, whereas PBS injected tumors failed to show any detectable autofluorescence

dx.doi.org/10.1021/bc3005304 | *Bioconjugate Chem.* 2013, 24, 1119−1133

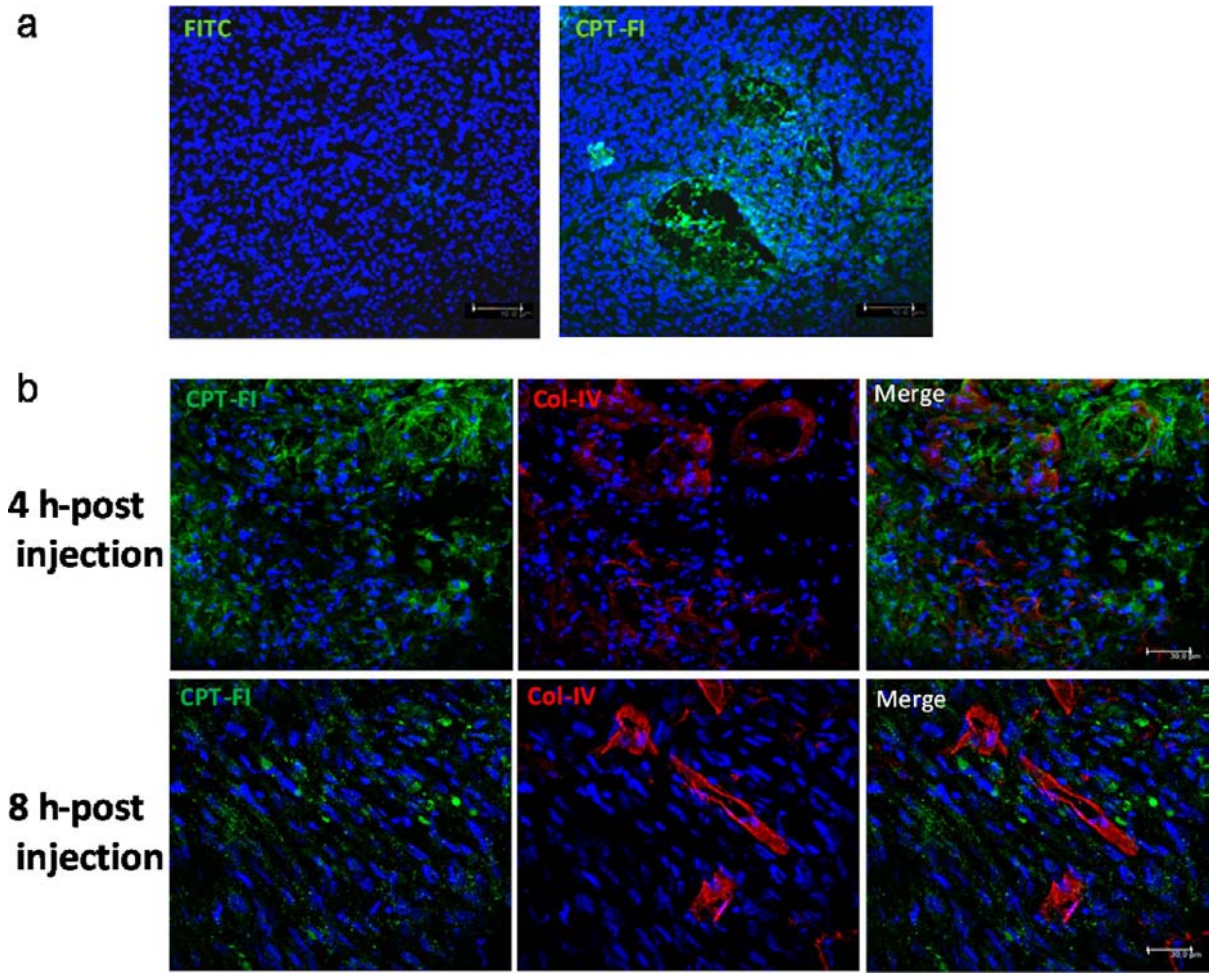

Figure 9. Fluorescent detection of CPT-FI in U87-forming tumors after intravenous administration in Nude mice. Tumor formation was assessed after subcutaneously inoculating 1×10^6 U87 into right flanks. Tumors reaching 300 mm^3 were treated *via* intravenous bolus injections of FITC ($n = 2$) or CPT-FI ($n = 3$). Mice received one intravenous injection of 100 μL FITC (A, 66 mg/kg) or CPT-FI (B, 66 mg/kg) through the tail vein. After 4 h postinjection, mice were sacrified and tumors were collected and frozen at −80 °C for postanalysis of fluorescence distribution. (a) Fluorescence images of glioma tumor cryosections showed no green fluorescence in FITC treated tumor and a marked parenchyma and perivascular green staining in the CPT-FI-treated tumor. (b) U87-bearing tumors corresponding to 4 and 8 h postinjections with CPT-FI were coimmunostained with an anticollagen IV antibody (Col-IV), in order to visualize the zones of neoangiogenic activity. DAPI, cell nuclei labeling in blue. Scale bar, 30 μm.

(Figure 8b). Deeper inside the tumor, some CPT-FI green zones would show cytotoxicity and diminished cell viability, and colocalization of the CPT-FI and DAPI stainings in isolated cells illustrates *in vivo* intranucleus incorporation (Figure 8c). Thus, confocal images of the CPT-FI distribution in consecutive sections show that only the tumor area exposed to CPT-FI injections is detectable, suggesting limited penetration of the drug. This restricted diffusion into the tumor may be due (i) to rapid uptake of the drug by perivascular cells and (ii) mostly to the cellular packing density and the number of adhesions between cells, as recently proposed.[34] Thus, intravenous administration strategy was employed to monitor the *in vivo* behavior of CPT-FI compared to FITC alone and to characterize tumor distribution. FITC (100 μL, $n = 2$) or CPT-FI (100 μL, $n = 3$) solutions at 66 mg/kg were bolus injected through the tail vein into Nude mice bearing U87 glioblastoma tumors. After 4 and 8 h, tumors were frozen and then analyzed. Confocal microscopic images were acquired 4 h after FITC or CPT-FI injection (Figure 9a). As expected, tumors did not show FITC signal whereas they exhibited very dense green staining in vascular and perivascular compartments after exposure to systemic CPT-FI (Figure 9a), and was mainly colocalized with collagen IV (Figure 9b). After 8 h, CPT-FI was not found with collagen IV immunostaining, and was more distributed throughout the glioma tumor parenchyma (Figure 9b). This data clearly indicate that CPT-FI can be delivered *via* intravenous injection, and that 8 h after administration, the labeled chemotherapy penetrated into the tumor parenchyma through the leaky tumoral vascular network, particularly dense in glioma tumors. Thus, it can be expected that this type of small tagged-anticancer molecules may be more widely dedicated to the study and the evaluation of pharmacokinetic, tumor penetration, and noncancerous sites of deleterious side effects.

CONCLUSIONS

In summary, we have described for the first time an original synthetic approach enabling the efficient fluorescent labeling of anticancer drug camptothecin which is known to exhibit a moderate chemical stability. The key point was the introduction of an azido-terminated linker onto the C10 position of the CPT quinoline ring, which acts as an optimal protecting group for the primary amino group only unveiled immediately prior to the final fluorescent labeling based on a peptide-type coupling reaction.

dx.doi.org/10.1021/bc3005304 | *Bioconjugate Chem.* 2013, 24, 1119−1133

Besides, careful functionalization at the C10 position of the pentacyclic alkaloid has shown to preserve the essential biological features of the CPT bioactive alkaloid, although longer incubation periods or higher concentrations are required. In addition, we demonstrated the feasibility of using a fluorescent topoisomease inhibitor CPT as a model drug to monitor in real-time cell *in vivo* delivery by fluorescent imaging inducing tumor senescence and arrest of cell growth. This new FI-tagged chemotherapy with similar characteristics as the CPT of interest will be very useful for continuous *in vivo* monitoring of a pseudo-drug upon externally triggered delivery. But mainly, the present aim was to open a new avenue of specific design of anticancer molecules as fluorescent probes, for the understanding of specific anticancer effects as well as nondesired effects including anemia, fatigue, or cognitive deficits commonly described in patients after chemotherapy.

■ ASSOCIATED CONTENT

Supporting Information

^{1}H and ^{13}C NMR data for all compounds and their HPLC chromatograph, and experimental details about photophysical characterization of CPT-FI. This material is available free of charge via the Internet at http://pubs.acs.org.

■ AUTHOR INFORMATION

Corresponding Author

*H.C.: e-mail helene.castel@univ-rouen.fr; phone + 33 (0)2 35 14 66 30. For C.S.: e-mail cyrille.sabot@univ-rouen.fr; phone + 33 (0)2 35 52 24 39.

Notes

The authors declare no competing financial interest.

■ ACKNOWLEDGMENTS

This work was supported by the Agence Nationale de la Recherche (Programme PIRIBio 2009, ANR "CLICKMAS-SLINK") for a postdoctoral fellowship to S.D., La Région Haute-Normandie via the CRUNCh program (CPER 2007-2013) and the CNRS. We thank Albert Marcual (COBRA - CNRS UMR 6014) for HRMS analyses, Annick Leboisselier (COBRA - CNRS UMR 6014, INSA de Rouen) for elemental analyses, and Laetitia Bailly (COBRA - CNRS UMR 6014, INSA de Rouen) for chiral HPLC analyses. Xavier Brune (Research master trainee, Université de Rouen, January-June 2012) is greatly acknowledged for his contribution to the large-scale synthesis of fluorescein-isonipecotic acid derivative **4**.

■ REFERENCES

(1) Wall, M. E., Wani, C. M., Cook, K. H., McPhail, A. T., and Sim, G. A. (1966) Plant antitumor agents. I. The isolation and structure of camptothecin, a novel alkaloidal leukemia and tumor inhibitor from Camptotheca acuminate. *J. Am. Chem. Soc. 88*, 3888−3890.

(2) Pommier, Y. (2009) DNA topoisomerase I inhibitors: chemistry, biology, and interfacial inhibition. *Chem. Rev. 109*, 2894−2902.

(3) Negoro, S., Fukuoka, M., Masuda, N., Takada, M., Kusunoki, Y., Matsui, K., Takifuji, N., Kudoh, S., Niitani, H., and Tagushi, T. (1991) Phase I study of weekly intravenous infusions of CPT-11, a new derivative of camptothecin, in the treatment of advanced non-small-cell lung cancer. *J. Natl. Cancer Inst. 83*, 1164−1168.

(4) Kawato, Y., Aonuma, M., Hirota, Y., Kuga, H., and Sato, K. (1991) Intracellular roles of SN-38, a metabolite of the camptothecin derivative CPT-11, in the antitumor effect of CPT-11. *Cancer Res. 51*, 4187−4191.

(5) Kingsburry, W. D., Boehm, J. C., Jakas, D. R., Holden, K. G., Hetch, S. M., Gallagher, G., Caranfa, M. J., McCabe, F. L., Faucette, L. F., Johnson, R. K., and Hertzberg, R. P. (1991) Synthesis of water-soluble (aminoalkyl)camptothecin analogs: inhibition of topoisomerase I and antitumor activity. *J. Med. Chem. 34*, 98−107.

(6) Gonçalves, M. S. T. (2009) Fluorescent labeling of biomolecules with organic probes. *Chem. Rev. 109*, 190−212.

(7) Middleton, R. J., and Kellam, B. (2005) Fluorophore-tagged GPCR ligands. *Curr. Opin. Chem. Biol. 9*, 517−525.

(8) Alonso, D., Vazquez-Villa, H., Gamo, A. M., Martínez-Esper, M. F., Tortosa, M., Viso, A., Fernandez de la Pradilla, R., Junquera, E., Aicart, E., Martín-Fontecha, M., Benhamú, B., Lopez-Rodríguez, M. L., and Ortega-Gutierrez, S. (2010) Development of fluorescent ligands for the human 5-HT1A receptor. *ACS Med. Chem. Lett. 1*, 249−253.

(9) Redy, O., and Shabat, D. (2012) Modular theranosticprodrug based on a FRET-activated self-immolative linker. *J. Controlled Release 164*, 276−282.

(10) Liu, Y.-Q., Dai, W., Tian, J. L., Yank, G., Feng, X.-W., Zhou, L., Kou, Y.-L., Zhao, W.-Q., Li, L.-H., and Li, H.-Y. (2011) Synthesis and insecticidal activities of novel spin-labeled derivatives of camptothecin. *Heteroat. Chem. 22*, 687−691.

(11) Gao, M., Miller, K. D., Sledge, G. W., and Zheng, Q.-H. (2005) Radiosynthesis of carbon-11-labeled camptothecin derivatives as potential positron emission tomography tracers for imaging of topoisomerase I in cancers. *Bioorg. Med. Chem. Lett. 15*, 3865−3869.

(12) Hinz, H. R., Harris, N. J., Giovanella, B. C., Ezell, E. L., and Liehr, J. G. (1996) Stabilities of 3H- and 2H-labelled camptothecins. *J. Label. Compd. Radiopharm.*, 733−742.

(13) Verma, R. P., and Hansch, C. (2009) Camptothecins: A SAR/QSAR Study. *Chem. Rev. 109*, 213−235.

(14) Devert, M., Sabot, C., Giboreau, P., Constant, J.-F., Greene, A. E., and Kanazawa, A. (2010) Total synthesis of (±)-17-norcamptothecin, a novel E-ring modified camptothecin. *Tetrahedron 66*, 7227−7231.

(15) Ziomkowska, B., Kruszewski, S., Siuda, R., and Cyrankiewicz, M. (2006) Deactivation rate of camptothecin determined by factor analysis of steady-state fluorescence and absorption spectra. *Optica Apllicata 1*, 137−146.

(16) Chourpa, I., Millot, J.-M., Sockalingum, G. D., Riou, J.-F., and Manfait, M. (1998) Kinetics of lactone hydrolysis in antitumor drugs of camptothecin series as studied by fluorescence spectroscopy. *Biochim. Biophys. Acta 1379*, 353−366.

(17) Kim, M., Ock, K., Cho, K., Joo, S.-W., and Lee, S. Y. (2012) Live-cell monitoring of the glutathione-triggered release of the anticancer drug topotecan on gold nanoparticles in serum-containing media. *Chem. Commun. 48*, 4205−4207.

(18) Weissleder, W., and Ntziachristos, V. (2003) Shedding light onto live molecular targets. *Nat. Med. 9*, 123−128.

(19) Fulmer, G. R., Miller, A. J. M., Sherden, N. H., Gottlieb, H. E., Nudelman, A., Stoltz, B. M., Bercaw, J. E., and Goldberg, K. I. (2010) NMR chemical shifts of trace impurities: common laboratory solvents, organics, and gases in deuterated solvents relevant to the organometallic chemist. *Organometallics 29*, 2176.

(20) Olmsted, J. (1979) Calorimetric determinations of absolute fluorescence quantum yields. *J. Phys. Chem. 83*, 2581−2584.

(21) Fang, F. G., Xie, S., and Lowery, M. W. (1994) Catalytic enantioselective synthesis of 20(S)-camptothecin: a practical application of the sharpless asymmetric dihydroxylation reaction. *J. Org. Chem. 59*, 6142−6143.

(22) Massif, C., Dautrey, S., Haefele, A., Ziessel, R., Renard, P.-Y., and Romieu, A. (2012) New insights into the water-solubilisation of fluorophores by post-synthetic "click" and Sonogashira reactions. *Org. Biomol. Chem. 10*, 4330−4336.

(23) Duan, Y., Liu, M., Sun, W., Wang, M., Liu, S., and Li, Q. X. (2009) Recent progress on synthesis of fluorescein probes. *Mini-Rev. Org. Chem. 6*, 35−43.

(24) Kobayashi, H., Ogawa, M., Alford, R., Choyke, P. L., and Urano, Y. (2010) New strategies for fluorescent probe design in medical diagnostic imaging. *Chem. Rev. 110*, 2620−2640.

(25) Comins, D. L., and Nolan, J. M. (2001) A practical six-step synthesis of (S)-camptothecin. *Org. Lett. 3*, 4255−4257.

(26) Gao, J., Wang, P., and Giese, R. W. (2012) Xanthamide fluorescent dyes. *Anal. Chem. 74*, 6397.

(27) Nadler, A., Hain, C., and Diederichsen, U. (2009) Histidine analog amino acids providing metal-binding sites derived from bioinorganic model systems. *Eur. J. Org. Chem.*, 4593−4599.
(28) Reddy, P. G., Pratap, T. V., Kumar, G. D. K., Mohanty, S. K., and Baskaran, S. (2002) The Lindlar catalyst revitalized: a highly chemoselective method for the direct conversion of azides to N-(tert-butoxycarbonyl)amines. *Eur. J. Org. Chem.*, 3740−3743.
(29) D'Arpa, P., and Liu, L. F. (1989) Topoisomerase-targeting antitumor drugs. *Biochim. Biophys. Acta 989*, 163−77.
(30) Friedman, H. S., Keir, S. T., and Houghton, P. J. (2003) The emerging role of irinotecan (CPT-11) in the treatment of malignant glioma in brain tumors. *Cancer*, 2359−62.
(31) Kim, C. Y., Lee, S. J., Kim, S. K., Park, C. K., Wang, K. C., and Cho, B. K. (2012) Antitumor activity of CKD-602, a camptothecin derivative, in a mouse glioma model. *J. Clin. Neuro. Sci. 19*, 301−305.
(32) Tanizawa, A., Kohn, K. W., Kohlhagen, G., Leteurtre, F., and Pommier, Y. (1995) Differential stabilization of eukaryotic DNA topoisomerase I cleavable complexes by camptothecin derivatives. *Biochemistry 34*, 7200−7206.
(33) Minchinton, A. I., and Tannock, I. F. (2006) Drug penetration in solid tumours. *Nat. Rev. Cancer 6*, 583−592.
(34) Grantab, R. H., and Tannock, I. F. (2012) Penetration of anticancer drugs through tumour tissue as a function of cellular packing density and interstitial fluid pressure and its modification by bortezomib. *BMC Cancer 12*, 214.